Available online at www.sciencedirect.com
ScienceDirect
Journal of Computational Physics 227 (2008) 6165–6183
JOURNAL OF COMPUTATIONAL PHYSICS
www.elsevier.com/locate/jcp

Optimization of energy confinement in the $1/\nu$ regime for stellarators

B. Seiwald [a,*], S.V. Kasilov [a,b], W. Kernbichler [a], V.N. Kalyuzhnyj [b], V.V. Nemov [a,b], V. Tribaldos [c], J.A. Jiménez [c]

[a] *Association EURATOM-ÖAW, Institut für Theoretische Physik – Computational Physics, TU Graz, Petersgasse 16, A–8010 Graz, Austria*
[b] *Institute of Plasma Physics, National Science Center "Kharkov Institute of Physics and Technology", Akademicheskaya Street 1, 61108 Kharkov, Ukraine*
[c] *Asociación EURATOM-CIEMAT, Madrid, Spain*

Received 16 May 2007; received in revised form 15 February 2008; accepted 21 February 2008
Available online 7 March 2008

Abstract

A set of powerful tools has been developed in the last years for the design of new stellarator devices. These codes, usually working in magnetic co-ordinates, comprise minimization of neoclassical transport, maximizing equilibrium and stability properties, etc. However, for certain conditions the stellarator magnetic field can be originally obtained in the real space coordinates and there is no necessity in its transformation to magnetic coordinates. Here a procedure working in real space co-ordinates is presented for maximizing the plasma energy content, based on reducing the most unfavorable, $1/\nu$, neoclassical transport. This tool is especially useful for existing stellarator devices which are not fully optimized with respect to neoclassical transport. Preliminary results for the "heliac-type" stellarator TJ-II are presented showing a configuration with almost twice the stored energy of the standard TJ-II configuration.

Keywords: Fusion plasma; Neoclassical transport; Optimization; Stellarator

1. Introduction

It has always been considered that the main disadvantage of stellarators is their rapid loss of high energetic particles and high neoclassical $1/\nu$ transport associated to their fully three dimensional magnetic field. The reason of these both phenomena is an enhanced ∇B drift of locally trapped particles across magnetic surfaces. However, recent theoretical, as well as computational, advancements have allowed to design new stellarators with superb neoclassical confinement properties, based on the concept of quasi-symmetry (see, e.g. [1–3]) or quasi-isodynamicity (see, e.g. [4–7]). The details of these configurations have been obtained through an

* Corresponding author. Tel.: +43 316 873 8194; fax: +43 316 873 8678.
E-mail address: seiwald@itp.tugraz.at (B. Seiwald).

0021-9991/$ - see front matter © 2008 Elsevier Inc. All rights reserved.
doi:10.1016/j.jcp.2008.02.026

optimization process in which different factors, weighting different physical or technical aspects of the device, are included. The usual starting point for such studies is the structure of the magnetic field, like imposing some type of quasi-symmetry, and thus most of numerical methods used are done in magnetic co-ordinates. Through an iterative process the physical goals are optimized and the feasibility of the coils is obtained by reversed engineering. These optimization techniques have shown to be so successful that it would be desirable to take advantage of them on existing devices in search for new operational regimes, or for evaluating possible upgrades. At the same time, for certain conditions the stellarator magnetic field can be originally obtained in real space coordinates and there is no necessity in its transformation to magnetic coordinates. In this case some advantages come into existence such as, e.g. the absence of the indicated transformation, the methods worked out for the transport study in real-space coordinates can be successfully used, taking into account the influence of magnetic islands and stochastic regions more easily and the possibility of more rapid analysis for complex configurations. Such an approach is applied to the analysis of the $1/\nu$ transport properties of stellarators in the present paper.

According to [8] among the various regimes of neoclassical transport just the $1/\nu$ transport should be optimized. For new optimized stellarators (e.g. HSX [9], NCSX [10,11], QPS [12,13]) conditions corresponding to low $1/\nu$ transport have been a design goal. For existing stellarators a certain decrease of this transport can be achieved by changes in coil currents (as it is done, e.g. for LHD).

In the present paper the $1/\nu$ transport properties of stellarators are analyzed by evaluating the energy content in the plasma. This content is increasing with decreasing transport coefficients. The energy confinement time which is connected to the energy content is one of the main characteristics of an experimental fusion device. As long as the core plasma is deeply in a collisionless regime the energy content is weakly sensitive to the temperature at the plasma boundary at large and, therefore, the influence of outer regions where the plateau or the Pfirsch-Schlüter regimes are important, is small. A relatively simple parameter like the energy content in the $1/\nu$ regime allows to limit the scope of optimization to the optimization of the magnetic field geometry which is, nevertheless, a demanding problem from computing time expense point of view.

So, optimizing the total stored energy in the plasma corresponds to optimizing the stellarator transport properties. For such an optimization the tool called SORSSA has been developed and is described in this paper. It is designed for optimizing stellarators with fixed coil design and allows to analyze improvements which can be done through changes of the coil currents (and/or coil positions). To calculate the necessary $1/\nu$ transport coefficients the field line integration technique [14] is used. The advantage of this technique is that the computations can be done for arbitrary stellarator magnetic fields using real space variables and all kinds of trapped particles are taken into account. With such an approach SORSSA optimizes the magnetic field produced by the coil currents of the device. Therefore, the optimization results are valid for the equilibria with a small plasma pressure or for devices with weak influence of the finite plasma pressure on the equilibrium magnetic configuration, e.g. for "heliac-type" devices like TJ-II [15]. These conditions allow for optimization fully in real space without any restrictions to the complexity of the magnetic field. This is in contrast to existing codes (e.g. [16] and [17]) for optimizing fusion devices in magnetic coordinates where MHD equilibrium codes (like VMEC [18]) are necessary.

We can assume that in TJ-II, for a sufficiently small β, the position and shape of the magnetic surfaces only slightly differ from those for the vacuum field and the neoclassical transport is approximately the same as for vacuum magnetic field. We can appeal to Refs. [1,8] in which it is pointed out that the properties of a stellarator configuration are completely determined by prescribing the shape of an outermost magnetic surface. When the magnetic field is given in magnetic coordinates, the neoclassical transport properties are linked with the structure of the magnetic field in those coordinates. However, in our approach it is not necessary to analyze this structure since the method [14] has been worked out for the direct calculation of the neoclassical transport coefficients in any stellarator magnetic field independently of the coordinate system and independently of the mod-B structure. The applicability of this method has been demonstrated in a number of works (see, e.g. [10,13,19]). At high β, in spite of a strongly helical magnetic axis the influence of the plasma pressure and the plasma currents can be manifested through the plasma position and shape, the variation of the rotational transform and the formation of magnetic islands. The correct evaluation of the bootstrap current is still an open question for devices like TJ-II because of large convergence problems in the long mean free path regime in DKES [20,21]. Monte Carlo techniques still are not able to give a reliable estimation of the bootstrap

current coefficients. In general, these effects only can be considered by means of three-dimensional MHD equilibrium codes such as VMEC, PIES [22], HINT [23,24]. Moreover, only the PIES and HINT codes can study magnetic island formation caused by finite β. But applying these two codes is really a very costly procedure. We cannot claim that the technique used in the present work is readily applicable to finite beta. However, it does provide magnetic configurations that are good candidates and also give a good indication of the potential improvement in the transport properties of the device.

The model for computing the total stored energy is presented in Section 2. A convenient definition of an effective radius of flux surfaces, as well as the detection of islands and stochastic zones are described there. The optimization scheme and the necessary adaption for the presented tool SORSSA are outlined in Section 3. In Section 4 an application to the "heliac-type" stellarator TJ-II [15] is presented. This device is well suited for this purpose, because it has a very high equilibrium beta, and therefore the plasma position and shape change very little with increasing beta. Preliminary computations of the stored energy for TJ-II have been done in Ref. [25]. And, finally, in Section 5 a conclusion is given.

2. Physics basis

Even in the most quiescent discharge a minimum level of randomly microscopic electromagnetic field fluctuations are present. These thermal fluctuations resulting from particle discreteness allow for a diffusive particle or energy loss. The corresponding minimal interactions are Coulomb collisions. These type of losses is irreducible (see, e.g. [26]). Compared to the classical transport theory for a magnetic field with straight field lines, the complication of the field configuration and hence more complex trajectories of particles in stellarators lead to a considerable increase in transport coefficients which is described by the neoclassical transport theory. Among various neoclassical transport regimes in stellarators, the so-called $1/\nu$ transport regime is the most unfavorable. Therefore, minimization of neoclassical transport in this regime is very important for stellarator transport optimization [8]. Lowering the $1/\nu$ transport even at zero electric field will have the beneficial effect of also lowering the associated transport rates in the presence of an electric field. For a simple model of the stellarator magnetic field the dependence of the $1/\nu$ transport on the magnetic field geometry is determined by the helical ripple [27]. In stellarators of general geometry the analogous dependence is usually considered by definition of an effective ripple (equivalent helical ripple), ϵ_{eff}, (see, e.g. in [28]). This means here that for a general stellarator magnetic field the transport coefficient can be presented in the same form as for the standard stellarator [27] just re-defining the amplitude of the ripple modulation. In this general case clearly, the magnetic field cannot be described by a single helical ripple harmonic. So, the $1/\nu$ neoclassical transport is measured by the effective ripple ϵ_{eff}, which is a function of the effective radius of the flux surface [14,25]. For good confinement properties ϵ_{eff} should be small. Assuming that neoclassical transport is dominant, the effective ripple can be used to compute the total stored energy in plasma by solving the heat conductivity equation using a given particle density profile (see Section 2.1). The radial dependence of ϵ_{eff} can be computed by a field line tracing code [14] where the magnetic field is directly computed from field coils without transformation to magnetic coordinates. Additionally, a proper detection of islands and ergodic zones has to be ensured (see Section 2.3).

Note that the $1/\nu$ neoclassical transport is considered here as the most unfavorable for energy transport. At the same time in the experiments the energy loss due to anomalous transport often dominates the neoclassical losses. However, in a number of experiments on W7-AS [29,30], CHS [31], LHD [32] with sufficiently high temperature of the plasma (higher than 1 keV) an increase of the neoclassical transport to the level or higher than the anomalous transport level has been observed. So, it can be expected that for sufficiently high plasma temperatures the neoclassical losses in neoclassically non-optimized stellarators are dominant because they strongly scale with the temperature.

2.1. Total stored energy

In stellarators in the presence of the radial electric field one possible scenario of neoclassical transport for thermonuclear parameters of the plasma is that the ions are not in the $1/\nu$ regime but in the ν or the $\sqrt{\nu}$ regimes because of their very small ion collision frequency. However, for electrons the collision frequency

is approximately 40 times higher than for ions and, therefore, electrons are often in the $1/\nu$ regime in this case. The plasma density fluxes are, in this case, small and correspond to ν or $\sqrt{\nu}$ regimes. However, the heat fluxes are determined in most cases by electrons and correspond to the $1/\nu$ regime. The role of the neoclassical electron heat transport in the $1/\nu$ regime has been discussed in, e.g. [27,29].

Let us consider flux surface averaged particle and energy densities carried by electrons which in the common literature (see, e.g. [28,21]) have the form:

$$F_{\mathrm{n}} = -n\left(D_{11}\left(\frac{1}{n}\frac{\partial n}{\partial r} + \frac{e}{T}\frac{\partial \Phi}{\partial r} - \frac{3}{2T}\frac{\partial T}{\partial r}\right) + D_{12}\frac{1}{T}\frac{\partial T}{\partial r}\right), \tag{1}$$

$$F_{\mathrm{W}} = -nT\left(D_{21}\left(\frac{1}{n}\frac{\partial n}{\partial r} + \frac{e}{T}\frac{\partial \Phi}{\partial r} - \frac{3}{2T}\frac{\partial T}{\partial r}\right) + D_{22}\frac{1}{T}\frac{\partial T}{\partial r}\right), \tag{2}$$

where (see Ref. [14])

$$D_{ij} = \frac{\sqrt{8}}{9\pi^{3/2}}\frac{v_{\mathrm{T}}^2\rho_{\mathrm{L}}^2}{\nu R_0^2}\epsilon_{\mathrm{eff}}^{3/2}\int_0^\infty \frac{\mathrm{d}z e^{-z}}{A(z)} z^{\frac{1}{2}+i+j}. \tag{3}$$

In accordance with the neoclassical transport theory (see, e.g. [27]) in the long mean free path conditions various regimes of the neoclassical transport can be realized dependently on the value the particle collision frequency ν. These are so called ν, $\sqrt{\nu}$ and $1/\nu$ regimes of transport. The ν and $\sqrt{\nu}$ regimes are realized in presence of radial electric field for smaller ν than the $1/\nu$ regime and their transport coefficients depend on the radial electric field. At the same time the most unfavorable regime for stellarators is the $1/\nu$ regime to which the presented paper is devoted. For this regime the positive role of the radial electric field is manifested in decreasing the width of the ν region of existence of this regime (increase of lower boundary in ν) and therefore in decreasing the maximum value of the diffusion coefficient. But directly the radial electric field does not enter into the transport coefficients for $1/\nu$ regime (see, e.g. [14,27]). However, equations for the particle flux and the heat flux for different species of particles contain the terms with this field. These terms allow to express the radial electric field corresponding to the ambipolar diffusion through the gradients of the particle density and the temperature. After that, using this expression, the ambipolar electric field can be eliminated from the expression for the fluxes.

In Eqs. (1)–(3) $v_{\mathrm{T}} = \sqrt{2T/m}$ is the thermal velocity, $\rho_{\mathrm{L}} = mcv_{\mathrm{T}}/(eB_0)$ is the mean Larmor radius, B_0 is a reference magnetic field, and R_0 is the major radius of the torus. The mean values of the collision frequencies ν (for electrons and ions) characterize the plasma behavior as a whole. These quantities are calculated for mean values of temperatures and particle densities (for electrons and ions). At the same time νA ($\nu A(v^2)$) is the pitch angle scattering frequency which depends on particle energy (characterizing not plasma but particle) (see [27,14]).

The effective ripple ϵ_{eff} (see also below), which is part of the $1/\nu$ neoclassical transport coefficients, takes into account particles being trapped within one magnetic field ripple as well as particles being trapped within several magnetic field ripples without restrictions to the complexity of the magnetic field [14]. This is an advancement to the standard neoclassical theory (see, e.g. [27,33,34]) where simplifications to the magnetic field were made and only particles trapped within single wells were taken into account.

In the following it is assumed that ions are cold and their transport coefficients are much smaller than those for electrons. Thus ion fluxes are put to zero. Due to the ambipolarity condition such $\partial\Phi/\partial r$ is established that the electron flux is equal to ion flux, what results in $F_{\mathrm{n}} = 0$. Estimating, with help of this condition and Eq. (1), gradients of n and Φ one obtains for the electron heat flux density

$$F_{\mathrm{W}} = -\kappa_\perp \frac{\partial T}{\partial r}, \tag{4}$$

where

$$\kappa_\perp = n\left(D_{22} - \frac{D_{12}D_{21}}{D_{11}}\right) = C_0\epsilon_{\mathrm{eff}}^{3/2}\frac{T^{7/2}}{B_0^2R_0^2}, \tag{5}$$

where C_0 is weakly (via Coulomb logarithm) dependent on device and plasma parameters.

The electron heat balance equation takes the form

$$\frac{\partial}{\partial t}\frac{3}{2}nT = \frac{1}{S}\frac{\partial}{\partial r}S\kappa_\perp\frac{\partial T}{\partial r} + Q(r), \tag{6}$$

where S is a magnetic surface area and $Q(r)$ is the flux surface averaged electron heat source. As it can be seen below, in case of TJ-II the shape of flux surfaces changes only little with radius and, therefore, S scales almost linearly with radius r, $S \approx 4\pi^2\alpha R_0 r$, where α is a factor depending on the shape of the flux surfaces. Considering steady-state and replacing S with r in (6) one gets

$$\frac{1}{r}\frac{\partial}{\partial r}r\kappa_\perp\frac{\partial T}{\partial r} + Q(r) = 0, \tag{7}$$

which is supplemented with the following boundary conditions

$$T(a) = 0 \quad \text{and} \tag{8a}$$

$$\lim_{r\to 0}\left(r\frac{\partial T}{\partial r}\right) = 0, \tag{8b}$$

where a is the plasma radius (this is either the radius of the last closed magnetic surface or of the last surface which does not intersect the wall). Assuming that the heat source is located at the magnetic axis,

$$Q(r) = \frac{P}{4\pi^2 R_0\alpha}\frac{\delta(r-\Delta)}{\Delta}, \quad \Delta \to +0, \tag{9}$$

where P is the input power. Integration of (7) from 0 to r and using (8b) gives

$$\kappa_\perp\frac{\partial T}{\partial r} + \frac{P}{4\pi^2 R_0\alpha r} = 0. \tag{10}$$

Substituting here (5), dividing the result by $\epsilon_{\text{eff}}^{3/2}$, integrating it from r to a and using (8a) gives

$$-\frac{2}{9}\frac{C_0}{B_0^2 R_0^2}T^{9/2}(r) + \frac{P}{4\pi^2 R_0\alpha}\int_r^a \frac{\mathrm{d}r'}{r'\epsilon_{\text{eff}}^{3/2}(r')} = 0, \tag{11}$$

or, explicitly

$$T = \frac{2r}{3S}P^{2/9}B_0^{4/9}R_0^{11/9}\left(\int_r^a \frac{\mathrm{d}r'}{r'\epsilon_{\text{eff}}^{3/2}(r')}\right)^{2/9} C, \tag{12}$$

where

$$C = 2^{1/3}3^{13/9}\pi^{14/9}\alpha^{7/9}C_0^{-2/9}.$$

Thus, one obtains for the total stored energy

$$W \equiv \int_0^a \mathrm{d}r S\frac{3}{2}nT = CP^{2/9}B_0^{4/9}R_0^{11/9}n_0\widehat{W} \tag{13}$$

with the normalized stored energy

$$\widehat{W} = \int_0^a \mathrm{d}r\, r\hat{n}(r)\left(\int_r^a \frac{\mathrm{d}r'}{r'\epsilon_{\text{eff}}^{3/2}(r')}\right)^{2/9} \tag{14}$$

and $\hat{n} = n/n_0$. The normalized stored energy is used for the optimization since the other quantities in Eq. (13) do not depend on coil currents or the effective radius and, therefore, stay constant during the optimization procedure. The integration variable in Eq. (14) is the effective radius of the magnetic flux surface as defined in Section 2.2. The effective ripple, ϵ_{eff}, contains the characteristic features of the magnetic field geometry.

In accordance with [14], the quantity $\epsilon_{\text{eff}}^{3/2}$ is represented as

$$\epsilon_{\text{eff}}^{3/2} = \frac{\pi R_0^2}{8\sqrt{2}}\lim_{L_s\to\infty}\left(\int_0^{L_s}\frac{\mathrm{d}s}{B}\right)\left(\int_0^{L_s}\frac{\mathrm{d}s}{B}|\nabla\psi|\right)^{-2} \times \int_{B_{\min}^{(\text{abs})}/B_0}^{B_{\max}^{(\text{abs})}/B_0}\mathrm{d}b'\sum_{j=1}^{j_{\max}}\frac{\hat{H}_j^2}{\hat{I}_j}, \tag{15}$$

$$\widehat{H}_j = \frac{1}{b'} \int_{s_j^{(\min)}}^{s_j^{(\max)}} \frac{\mathrm{d}s}{B} \sqrt{b' - \frac{B}{B_0}} \left(4\frac{B_0}{B} - \frac{1}{b'} \right) |\nabla\psi| k_{\mathrm{G}}, \tag{16}$$

$$\widehat{I}_j = \int_{s_j^{(\min)}}^{s_j^{(\max)}} \frac{\mathrm{d}s}{B} \sqrt{1 - \frac{B}{B_0 b'}}. \tag{17}$$

This quantity is computed by integration over the magnetic field line, s, over a sufficiently large interval $0 - L_{\mathrm{s}}$, and by integration over the perpendicular adiabatic invariant of trapped particles, $J_\perp$. Here, $B_{\min}^{(\mathrm{abs})}$ and $B_{\max}^{(\mathrm{abs})}$ are the minimum and maximum values of B within the interval $[0, L_{\mathrm{s}}]$. The quantities $s_j^{(\min)}$ and $s_j^{(\max)}$ within the sum over j in (15)–(17) correspond to the turning points of trapped particles. This integration takes into account all kinds of trapped particles, such as those trapped within one magnetic field ripple as well as particles trapped within several magnetic field ripples. The geodesic curvature of the magnetic field line, which is given as $k_{\mathrm{G}} = (\mathbf{h} \times (\mathbf{h} \cdot \nabla)\mathbf{h}) \cdot \nabla\psi / |\nabla\psi|$ with the unit vector $\mathbf{h} = \mathbf{B}/B$.

In case of Boozer magnetic coordinates [35] the gradient of the flux surface label $\nabla\psi$ is calculated using the Boozer spectra of the coordinates of the magnetic surfaces (see Refs. [14,36]). In the present work computations are done in real space coordinates namely, in cylindrical coordinates $\xi^i = (R, Z, \varphi)$, and $\nabla\psi$ is calculated using integration along the magnetic field line of the equations for the vector $\mathbf{P} \equiv \nabla\psi$ (see Refs. [37,14])

$$\frac{\mathrm{d}P_i}{\mathrm{d}s} = -\frac{1}{B} \frac{\partial B^j}{\partial \xi^i} P_j, \tag{18}$$

where B^j are the contra-variant components of $\mathbf{B}$ in real-space coordinates ξ^i, and $P_j = \partial\psi/\partial\xi^j$ are the covariant components of $\mathbf{P}$.

The magnetic field is computed directly from coil parameters with the use of a Biot–Savart code.

2.2. Effective radius of a magnetic surface

The effective radius of a magnetic flux surface is defined in [14] in differential form, $S\mathrm{d}r = \mathrm{d}V$, where S is the area of the magnetic surface and V is the volume enclosed by that magnetic surface. In this case, the computation r requires the calculation of many magnetic surfaces. The accuracy is low if just a few surfaces are used. To overcome this problem, a different definition of an effective radius $r_{\mathrm{eff}} = 2V/S$, which can be calculated during a single field line integration, is introduced. Dividing the volume V, limited by the magnetic surface, by the surface area S, one obtains

$$r_{\mathrm{eff}} \equiv \frac{2V}{S} = \frac{2}{3} \frac{\int \mathrm{d}S \mathbf{r} \cdot \frac{\nabla\psi}{|\nabla\psi|}}{\int \mathrm{d}S} = \frac{2}{3} \frac{\langle \mathbf{r} \cdot \nabla\psi \rangle}{\langle |\nabla\psi| \rangle} = \frac{2}{3} \lim_{L_s \to \infty} \frac{\int_0^{L_s} \frac{\mathrm{d}s}{B} \mathbf{r} \cdot \nabla\psi}{\int_0^{L_s} \frac{\mathrm{d}s}{B} |\nabla\psi|}, \tag{19}$$

where $\nabla\psi$ is the vector normal to the flux surface, $\mathbf{r}$ is a radius vector, B the module of the magnetic field and $\mathrm{d}s$ a distance measured along the magnetic field line. Formally the effective radius can take negative values if the gradient at the starting point is inward directed. The definition (19) is used in Eq. (14) for the optimization.

The computation of the normal vector $\nabla\psi$ during the field line integration can be done if its direction is known at the beginning of the integration (see [37]). The direction of $\nabla\psi$ is given at $Z = 0$ in the $\varphi = 0$ plane due to symmetry properties of the magnetic flux surface in this point. With the choice $|\nabla\psi| = 1$ at this point, the flux surface label ψ coincides with R_{beg} up to an additive constant, where R_{beg} is a starting value of R. Of course, if ψ is replaced with any other monotonous function of ψ, this has no effect on the results.

The effective radius (19) is close to the same quantity defined in [14], since the effective ellipticity of the cross-sections of magnetic surfaces changes not significantly with the radius. Therefore, it is convenient to use such a definition of a radius which can be computed for each field line during the field line integration. A comparison of both definitions of the radius this is shown for TJ-II in Fig. 1.

For integrating Eq. (14) it is necessary to keep track of regions with field lines being: (i) stochastic, (ii) close to rationals, or (iii) intercepted by the vacuum vessel, or (iv) forming islands. For these field lines the label "inappropriate" will be used.

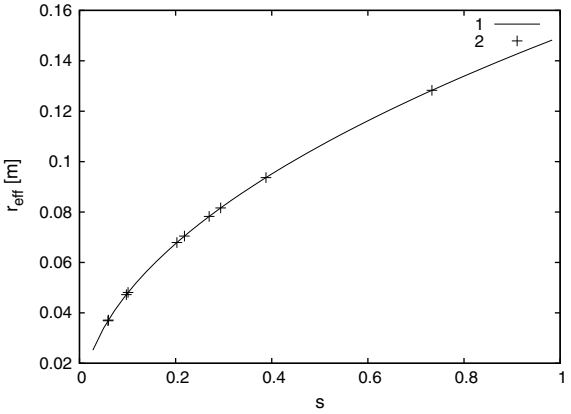

Fig. 1. The effective radius calculated as proposed in [14] (solid line) compared to the effective radius as proposed in Eq. (19) with the field line integration (crosses) for the TJ-II "standard" configuration.

2.3. Detection of islands and inappropriate field lines

The effective radius of nested magnetic surfaces increases from the magnetic axis towards the plasma boundary. The effective radius of a magnetic island is very small compared to the radius of neighboring magnetic surfaces (see Fig. 2). In Fig. 2 the island appears at $R_{\mathrm{beg}} = 1.643$ m. The computed effective radius of the island is $r_{\mathrm{eff}} = -0.009$ m (see explanation after formula (19)), which is considerably smaller than the effective radius of the neighboring flux surfaces with absolute values of their effective radius of about 0.11 m and 0.13 m. An example where the island chain appears close to the last closed magnetic surface is given in Fig. 3.

The integration of Eq. (14) is done with respect to r_{eff}. As can be seen from Fig. 2, the effective radius is not continuously increasing when islands are taken into account, so islands have to be detected and excluded from integration of Eq. (14).

The detection of magnetic islands is done in the $\varphi = 0$ plane. For this purpose the angle α between the vectors $\mathbf{r}_g$ and $\nabla\psi$ is used (see Fig. 4). The vector $\mathbf{r}_g$ points from the magnetic axis (MA) to a point on the magnetic surface. The magnetic axis is the innermost (degenerated) magnetic surface with $r_{\mathrm{eff}} = 0$. For any magnetic surface cos α has the same sign (negative in our case) for all points on the surface. If the magnetic axis is not located inside the flux surface, like for magnetic islands, the numbers of positive and negative values for cos α are close to each other.

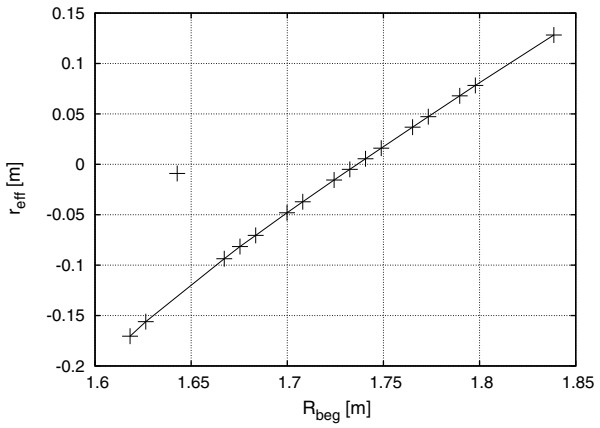

Fig. 2. Finding the magnetic axis for the standard configuration of the TJ-II in the $\varphi = 0$ plane. The point at $R_{\mathrm{beg}} = 1.643$ m with $r_{\mathrm{eff}} = -0.009$ m belongs to an island and is not used for finding the magnetic axis.

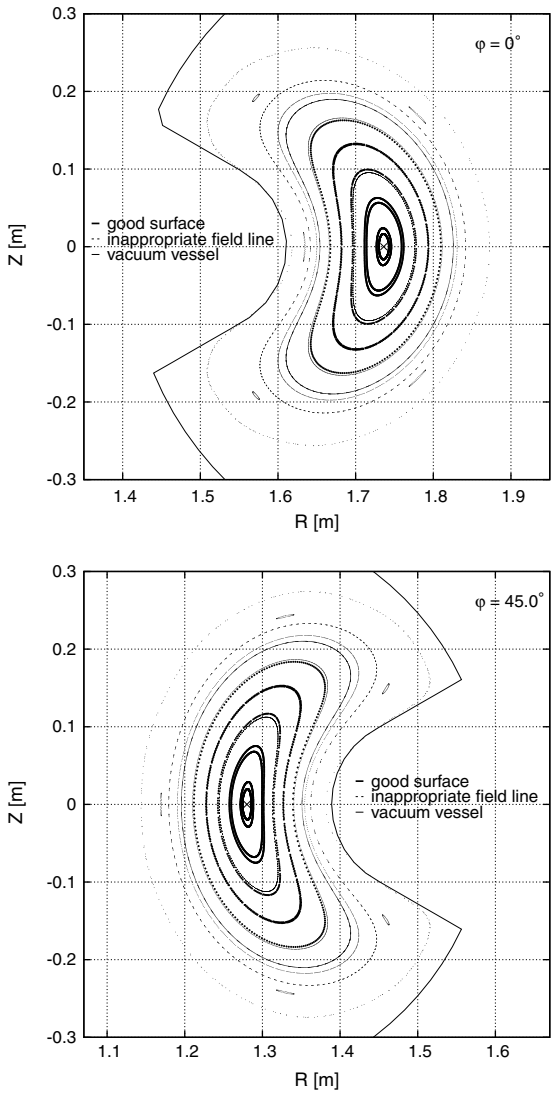

Fig. 3. Cross sections of the TJ-II standard configuration. Only the "good surfaces" are used for computation of the stored energy, field lines labeled with "inappropriate field line" are not used. Error codes are used for field lines forming stochastic zones or islands, touching the vacuum vessel or where the maximum number of periods for integration is exceeded.

The magnetic axis is found by fitting the effective radius r_{eff} vs. the initial value R_{beg} for the field line integration (see Fig. 2). For the magnetic axis, as mentioned above r_{eff} is zero. For fitting $r_{\text{eff}}(R_{\text{beg}})$ only the nested flux surfaces can be used, therefore, islands have to be excluded.

The normal vector $\nabla\psi$ is sensitive to islands close to a magnetic surface. For this flux surface $\nabla\psi$ shows a characteristic convexity. This is shown in Fig. 5. The island 1 (Fig. 5a) close to the surface 2 (Fig. 5b) cause small "bumps" in the distribution of $\nabla\psi$ over the surface which are not seen in case of surface 3.

Field lines which belong to a stochastic zone do not form a magnetic surface. For such field lines the module of $\nabla\psi$ increases continuously. This behavior can be explained by the fact that, in this case, the function ψ (as well as $\nabla\psi$) is not a single valued function of the position. These field lines can be easily marked as "inappropriate".

Field lines, which form islands, belong to a stochastic zone or to a zone where the rotational transform ι (for definition see Eq. (27)) is close to a rational number are not used for computations of the total stored

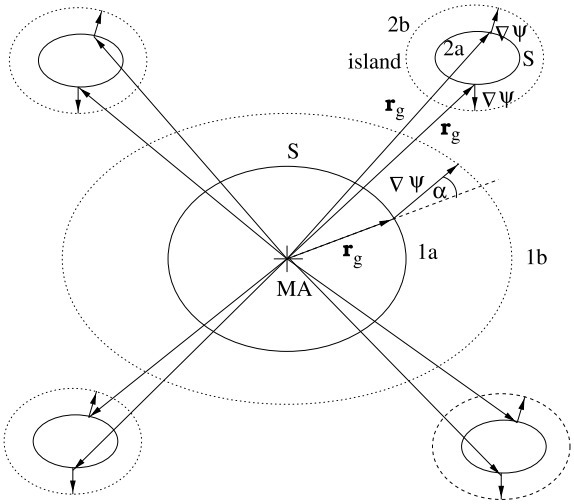

Fig. 4. Island detection: Here a flux surface 1a and an island 2a corresponding to $\iota = 1/4$ are shown. The corresponding shapes of the normal vector $\nabla\psi$ to the flux surface and the island are labeled with 1b and 2b. *MA* denotes the magnetic axis and *S* the magnetic surface.

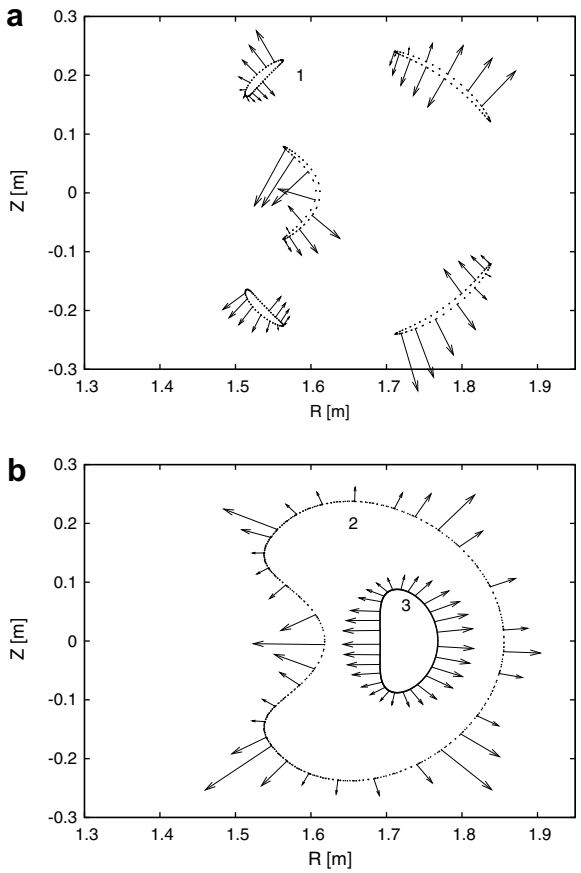

Fig. 5. Flux surfaces and the corresponding $\nabla\psi$ for some points on the flux surfaces (see also Fig. 4) for an island chain (a) and two flux surfaces (b).

energy. Nevertheless, they are shown in the plots of cross sections to present a picture as realistic as possible. The unused field lines are marked with "inappropriate field line".

Note that the impact on confinement of zones with magnetic islands and with field lines termed as "inappropriate" is negative. Because of the big longitudinal heat conductivity the temperature gradient in such zones is negligible. Therefore, for the intervals of r corresponding to such zones in Eq. (7) the T value is taken to be constant.

3. Optimization procedure

The optimizer uses the Simulated Annealing (SA) algorithm, which is a stochastic method for optimization and first presented by Kirkpatrik et al. [38]. It is used for solving combinatorial optimization problems and has been proven to be a good technique for numerous applications [39,40]. In the following subsection the Simulated Annealing algorithm, as it is used, is summarized.

3.1. Theoretical basis of the Simulated Annealing algorithm

The idea behind the SA algorithm is borrowed from thermodynamics and models the way liquids crystallize and freeze during an annealing process. When the temperature is high the particles can move freely. The high kinetic energy enables the particles to overcome the differences of potential energies of various configurations. Cooling down a liquid slowly causes a loss of mobility and an ordering process is achieved. If the result is an ideal crystal, the cost function (free energy) attains its absolute minimum. If the cooling process is too fast, the system achieves a non ideal state and ends up in a local minimum (which corresponds to a polycrystalline or amorphous state). As it is of interest to find the global minimum, a slow cooling process is simulated. An artificial temperature T and a probability distribution $p_{\mathrm{E}}(\mathbf{x}_{\mathrm{t}}|T)$, the so called acceptance distribution for a given configuration $\mathbf{x}$ and a given temperature T, are introduced. The cost function, which is to be minimized, is denoted by $E(\mathbf{x})$ and can depend on a set of either discrete or continuous variables $\mathbf{x}$. It is set to

$$p_E(\mathbf{x}_{\mathrm{t}}|T) = \frac{1}{Z}\mathrm{e}^{-(E(\mathbf{x})-E_{\min})/T} \tag{20}$$

which corresponds to a Boltzmann distribution with a normalization factor Z. Note, that the knowledge of $E_{\min}$ is not really required, because this factor can be absorbed in Z. The distribution p_{E} has a high probability for states $\mathbf{x}$ with a low value for $E(\mathbf{x})$. Close to the optimum states a random walk approach would take a long time.

An implementation of SA requires the following three steps:

(1) Generation of states.
(2) Acceptance of states.
(3) A cooling scheme.

ad 1: Generation of states In the vicinity of the current state $\mathbf{x}_{\mathrm{n}}$ (n is the step index) a trial point $\mathbf{x}_{\mathrm{t}}$ is chosen randomly. The trial point is within a sphere around $\mathbf{x}_{\mathrm{n}}$ with a radius σ. When the temperature is lowered, σ is reduced too.

ad 2: Acceptance of states For a chosen $\mathbf{x}_{\mathrm{t}}$ the acceptance probability

$$q = \min\left\{1, \frac{p_{\mathrm{E}}(\mathbf{x}_{\mathrm{t}}|T)}{p_{\mathrm{E}}(\mathbf{x}_{\mathrm{n}}|T)}\right\} \tag{21}$$

governs the acceptance of $\mathbf{x}_{\mathrm{t}}$. The new state is accepted as $\mathbf{x}_{\mathrm{n}+1}$ if $q = 1$, otherwise a pseudo random number r is created. If $r \leqslant q$ the new state $\mathbf{x}_{\mathrm{t}}$ is accepted as $\mathbf{x}_{n+1}$ otherwise the old state is kept $\mathbf{x}_{\mathrm{n}+1} = \mathbf{x}_n$ for the next step. This enables a possibility for leaving a local minimum.

ad 3: Cooling scheme A proper choice of a initial temperature T_0 is an important first step. The initial temperature

$$T_0 = \sqrt{\langle (\delta E)^2 \rangle (\infty)} \tag{22}$$

is used, where $\langle (\delta E)^2 \rangle (\infty)$ is the variance of the energy (cost function) at $T = \infty$. The criterion for T_0 ensures that $E(T_0)$ lies just within the area of fluctuations of $\langle (\delta E)^2 \rangle (\infty)$.

For a proper cooling strategy it is required that the probability of acceptance for two consecutive temperatures T_k and T_{k+1} differs by a sufficiently small amount. This is achieved if

$$\frac{1}{1+\delta} < \frac{p_E(\mathbf{x}|T_k)}{p_E(\mathbf{x}|T_{k+1})} < 1 + \delta \tag{23}$$

with $\delta \ll 1$. Using the Boltzmann distribution T_{k+1} is obtained as

$$T_{k+1} = \frac{T_k}{1 + \frac{T_k}{3\sqrt{\langle (\delta E)^2 \rangle}} \ln(1+\delta)}. \tag{24}$$

The advantage of this scheme compared to the simple $T_k = T_0 q^k$ with e.g. $q = 0.95$ is, that phase transitions are automatically taken into account and the temperature there is lowered slowly. Close to phase transitions, fluctuations are rather large and the simulation could end up in a configuration far away from the optimum configuration. If the simple cooling scheme is used, the probability to end up in such a configuration is higher than for the cooling scheme (24).

Finally, it has to be detected when the simulation has converged, meaning that the current temperature T_k has reached the end temperature T_e. SA has converged if the expectation value $\langle E \rangle (T_e)$ differs from the optimal value $E_{\min}$ only by a sufficiently small value ε. This is expressed as

$$\frac{\langle E \rangle (T_e) - E_{\min}}{\langle E \rangle (T_0) - \langle E \rangle (T_e)} < \varepsilon \tag{25}$$

which results in the criterion

$$\frac{\langle (\delta E)^2 \rangle (T_e)}{T_e (\langle E \rangle (T_0) - \langle E \rangle (T_e))} < \varepsilon. \tag{26}$$

As cost function for the optimization procedure $E = -\widehat{W}$ is used, since the goal is to find a maximum of $\widehat{W}$. The proper computation of the normalized stored energy $\widehat{W}$ is a key feature of the optimization code designed for improving existing devices through (minor) changes in coil currents (and/or coil positions) [25,41].

3.2. Problem specific

For computing the normalized stored energy with help of Eq. (14) it is necessary to compute the effective ripple ϵ_{eff} (Eq. (15)) and the effective radius (Eq. (19)) for a certain amount of flux surfaces. As already mentioned in previous sections, only good field lines forming good flux surfaces (this are field lines which are not labeled as inappropriate) can be used.

For a good estimation of the normalized stored energy approximately 20 good flux surfaces are necessary. As it is not possible at the start of SORSSA runs to know about the number of inappropriate field lines, a fixed number of field lines which are computed is used. For interesting configurations could be seen, that the number of inappropriate field lines is less than 1/3 of the computed field lines within the plasma boundary. Consequently, 30 field lines are computed within the plasma boundary. The interception by the vacuum vessel and the stochasticity of a field line are detected during the integration. The detection of islands is done after computation of all field lines, because the estimation of the magnetic axis is needed (see Section 2.3).

It has been seen, that for a good estimation of the effective ripple ϵ_{eff} at least 200 field periods have to be integrated. For stopping the field line integration a simple criterion is used – the field line should cover the flux surface equally.

If the rotational transform ɨ, defined in toroidal geometry as $\text{ɨ} = \iota/2\pi$ with

$$\iota \equiv \lim_{n\to\infty} \frac{m}{n} = \lim_{\varphi\to\infty} \frac{\theta(\varphi)}{\varphi}, \tag{27}$$

where φ is the angle of the toroidal rotation and θ the angle in poloidal direction, is close to a rational number, the field line covers the flux surface not equally. This means that the points at the cross sections are "blocked" and not equally distributed (see Fig. 6). As a consequence, for covering the flux surface equally with the field line, a large number of periods have to be followed for determining good values for ϵ_{eff} and r_{eff}. As this is of big disadvantage for a optimization, field lines are inappropriate and integration is stopped if a limit of 2000 periods for integration is exceeded.

3.3. Acceleration of the procedure

The computational time for integrating a sufficient number of field lines for a magnetic field configuration is very high. So it is desirable to speed up the computations.

As stated in the last paragraph of the Introduction TJ-II is well suited for SORSSA. In principle, finite β actually matters and in general β should be taken into account. It would be necessary to run MHD codes and check the performance of finite plasma pressure after optimizing vacuum configurations (and perhaps if necessary iterate the whole process). Because of the peculiarities of TJ-II and its stiffness with respect to β this method is not necessary for TJ-II. Magnetic field lines can be computed independently from each other. Therefore, it is possible to parallelize the computation of magnetic field lines. For this purpose the Message Passing Interface (MPI) [42,43], a very flexible system, has been chosen. For SORSSA a master/slave model has been implemented. The master process executes the Simulated Annealing algorithm and computes $\widehat{W}$ according to Eq. (14). The integrations of the field lines are done by the slave processes, which send (among other data) $\epsilon_{\text{eff}}^{3/2}$ to the master process. The main advantage of this method for speeding up the computation is that the calculation of the total stored energy for one configuration on multiprocessor systems or clusters of computers is very fast as it is done in parallel.

For further reduction of the computational time a relatively standard multi grid method is implemented. For the computations only discrete values of the coil currents (and coil positions) are used. This means that a grid is spanned over the parameter space defined by all variable quantities. The grid size is chosen in a way that the total stored energy in plasma does not change excessively from one grid point to a neighboring one, so the function will not artificially become too spiky. A proper grid size is determined by performing preliminary scans.

If an interesting maximum of $\widehat{W}$ is found, the optimization is started at this maximum or close to it with a substantially refined grid and a reduced allowed parameter space to further resolve this maximum.

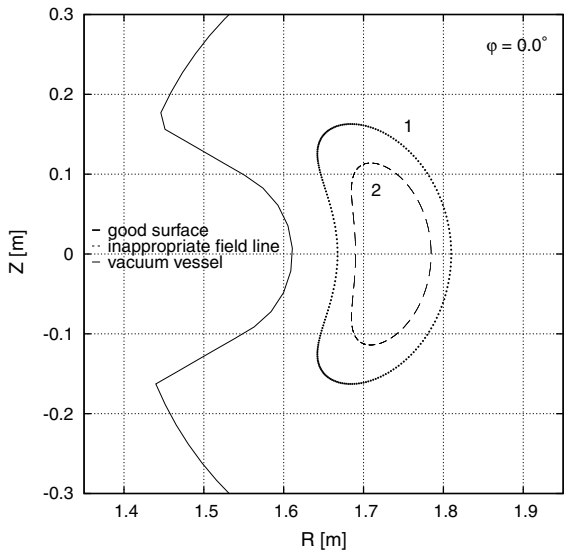

Fig. 6. Comparison of a "good surface" (1) with a flux surface (2) with a near rational ι (defined in Eq. (27)) of the TJ-II standard configuration.

Furthermore, all computed configurations are stored in a proper data structure in a database for restarts of the optimizer. Therefore, it is not necessary to compute the same configuration twice.

With the methods for accelerating, described in this section, the time for computing the normalized stored energy for one configuration is reduced to approximately 20 minutes when using 20 processors (Intel Xeon CPU with 2.66 GHz) for computation of 30 field lines.

4. Application to TJ-II heliac-type stellarator

It is desirable to try to improve the neoclassical $1/\nu$ transport properties for the stellarator TJ-II [44] (see Fig. 7). SORSSA is used to look for TJ-II configurations with enhanced energy confinement compared to the TJ-II standard configuration with respect to neoclassical $1/\nu$ transport properties as described in Section 2. Calculations are performed in real space without changing the shape and position of the coils, but just by varying the currents flowing in the coils of the already built device. Note that in magnetic coordinates for the analogous purposes the STELLOPT [12] package from ORNL can be used.

The stellarator TJ-II is a medium size heliac ($R = 1.5$ m, $a < 0.2$ m) with four field periods. The free parameters for the "common" TJ-II operation are (1) the toroidal coil current, (2) the current for the helical winding, (3) the current for the central circular coil and (4) the current for vertical field coils. The coil system consists of one central circular coil, two vertical field coils, 32 toroidal coils, which are helically displaced, and one central helical coil wrapped around the central circular coil (following the winding law of the toroidal coils). The

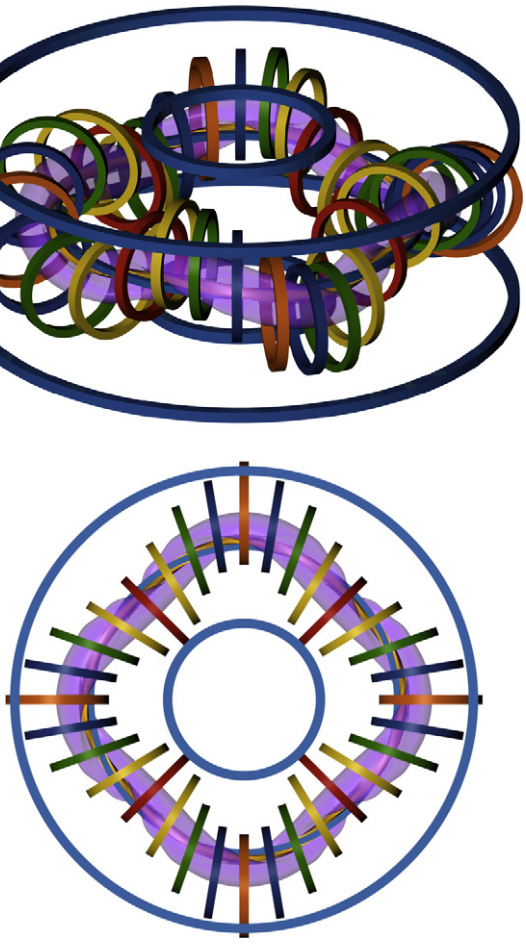

Fig. 7. Sketch of the TJ-II coil configuration.

toroidal coils are responsible for the main magnetic field ($B_0 \approx 1$ T). SORSSA offers the possibility to estimate the quality of the $1/v$ neoclassical transport properties using real space coordinates. The main drawback is that only vacuum configurations can be computed. This is not a severe problem, at least for TJ-II, because of its stiffness with respect to β, as mentioned in Section 3.3.

The effective helical ripple ϵ_{eff} is valid only in the $1/v$ long mean free path (lmfp) regime and for small enough radial electric field such that angular velocity of poloidal rotation due to the electric drift is small compared to effective collision frequency of electrons.

For a run of the optimizer the toroidal coil current, the current for the helical winding, the current for the central circular coil and the current for vertical field coils are varied. The range of their variation is $\pm 20\%$ of the corresponding values for the standard configuration, which is within the technical constraints. For the particle density a constant profile is used.

Poincaré cuts of the field lines of the standard configuration at $\varphi = 0$ and at half of the period are shown in Fig. 3. The corresponding value of the total stored energy is $\widehat{W} = 0.97 \cdot 10^{-2}$. An improvement of the total stored energy is obtained either by an increase of the plasma volume or a reduction in neoclassical transport

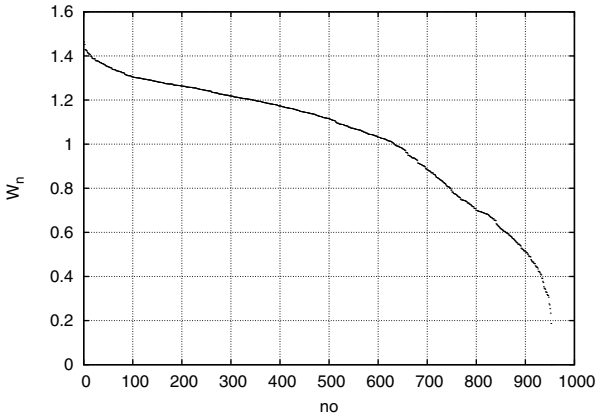

Fig. 8. The re-normalized stored energy vs. number of configuration for the considered TJ-II configurations (see Eqs. (14) and (28)).

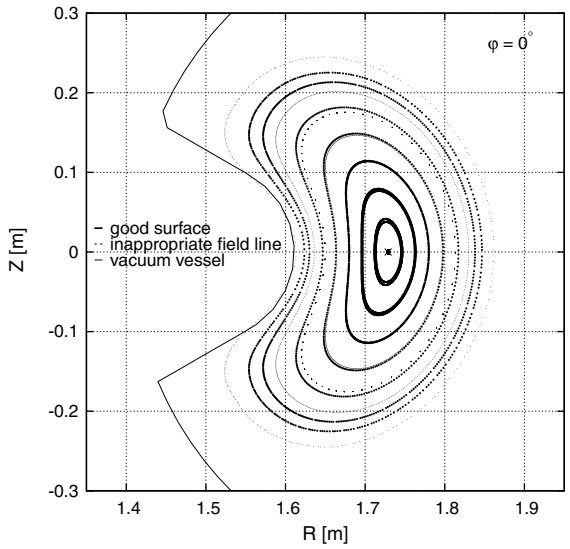

Fig. 9. Cross section of the "best" TJ-II configuration with enhanced total stored energy as compared to the standard configuration.

or both. In the frame of these studies several configurations with enhanced stored energy could be found. This can be seen in Fig. 8 where the re-normalized stored energy

$$W_{\mathrm{n}} = \widehat{W}/\widehat{W}_S, \tag{28}$$

with $\widehat{W}$ taken from Eq. (14) and the normalized stored energy of the TJ-II standard configuration $\widehat{W}_S$, is shown for the considered configurations. Only for the very best configurations the total stored energy is increased due to an increase of the plasma volume and a reduction in neoclassical transport. For the majority of the considered configurations the plasma volume is improved and the neoclassical transport is increased or vice versa. For the worst configurations a strongly reduced plasma volume and a strongly increased neoclassical transport is observed. In order to illustrate the effect of neoclassical transport and plasma volume on confinement three selected computed cases are presented and discussed in the following.

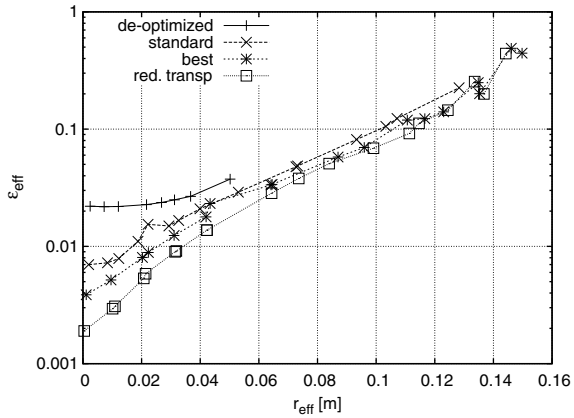

Fig. 10. Effective ripple $\epsilon_{\mathrm{eff}}^{3/2}$ vs. effective radius r_{eff} for TJ-II configurations: "de-optimized", standard, "best" and "red. transp." with a markedly reduced effective ripple.

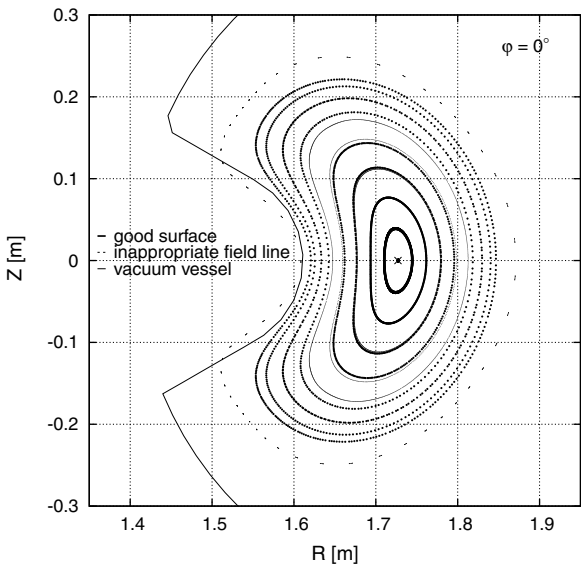

Fig. 11. Cross section of the "red. transp." TJ-II configuration with enhanced total stored energy but reduced plasma volume as compared to the "best" configuration.

The first configuration, hereafter referred as "best" configuration, shown in Fig. 9 does not exhibit an island structure close to the vacuum vessel (like the TJ-II standard configuration), which limits the plasma volume. Moreover, as can be seen on Fig. 10, the value of the effective ripple for the "best" configuration is significantly smaller than for the standard configuration. Consequently, the total stored energy in the "best" configuration, $\widehat{W} = 1.41 \cdot 10^{-2}$, is higher as compared to the standard configuration, representing an increase of ≈45%. The second configuration is shown in Fig. 11 and is referred as "red. transp." configuration. It exhibits a slightly smaller plasma volume but with an even more reduced transport than in the "best" configuration, as can be seen in Fig. 10. For the "red. transp." configuration the stored energy is found to be $\widehat{W} = 1.38 \cdot 10^{-2}$, which is obviously a lesser performance then for the "best" configuration, although better than the standard configuration. The "de-optimized" configuration, shown in Fig. 12, represents an extreme case of low plasma volume and high transport (see Fig. 10) with, as a consequence, very poor confinement, $\widehat{W} = 0.18 \cdot 10^{-2}$.

Another interesting quantity for characterizing configurations presented above can be to compare their respective rotational transform ɨ, defined in Eq. (27). The rotational transform profiles (see Fig. 13) are flat

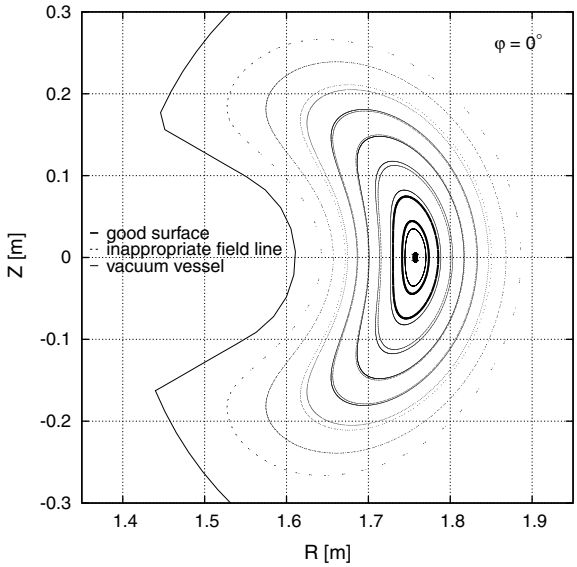

Fig. 12. Cross section of the "de-optimized" TJ-II configuration with low plasma volume and high neoclassical transport.

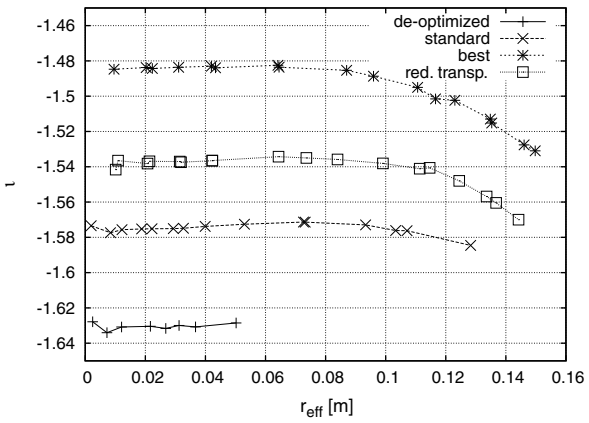

Fig. 13. Rotational transform ɨ vs. effective radius r_{eff} for TJ-II configurations: "de-optimized", standard, "best" and "red. transp.".

from the magnetic axis to about $r_{\mathrm{eff}} \approx 8$ cm, which is roughly half of the plasma radius, and then increase slightly towards the plasma edge (note, the plasma radius of the "de-optimized" configuration is $a \approx 5$ cm). For the "de-optimized" configuration ι is close to -1.63.

5. Conclusion

SORSSA, a tool for optimizing stellarators in real space coordinates, has been successfully applied to the heliac-type stellarator TJ-II. From the various configurations with enhanced stored energy which have been found, three characteristic ones have been presented to illustrate the influence of neoclassical transport in the $1/\nu$ regime and of plasma volume on confinement. Among those, a configuration with reduced transport and, at the same time, increased plasma volume, as compared to the standard configuration, was shown to have an increase in total stored energy of approximately 45% compared to the TJ-II standard configuration. The same increase of the stored energy for the standard configuration would require, according to the scaling law (13), 5.3 times higher input power P.

The optimization tool for stellarators, SORSSA, has shown that TJ-II vacuum configurations can be improved in terms of neoclassical transport. Nevertheless some more investigations are desirable, e.g. to ensure that configurations with enhanced stored energy are good operating points.

In principle it is also possible to modify SORSSA for fast checking of new and simple coil configurations, e.g. if mainly circular, planar coils are considered. For such applications the positions and radii of coils would be varied, in addition to coil currents, during an optimization run.

Acknowledgment

This work, supported by the European Communities under the contract of Association between EURATOM and the Austrian Academy of Sciences, was carried out within the framework of the European Fusion Development Agreement. The views and opinions expressed herein do not necessarily reflect those of the European Commission. It should also be acknowledged that this work has been carried out with funding from the Austrian Science Fund (FWF) under contract No. P16797-N08.

References

[1] J. Nührenberg, R. Zille, Quasi-helically symmetric toroidal stellarators, Phys. Lett. A 129 (2) (1988) 113–117.
[2] D.A. Garren, A.H. Boozer, Existence of quasihelically symmetric stellarators, Phys. Fluids B 3 (10) (1991) 2822–2843.
[3] M. Yu. Isaev, M.I. Mikhailov, V.D. Shafranov, Quasi-symmetrical toroidal magnetic systems, Plasma Phys. Rep. 20 (4) (1994) 319–335.
[4] M.I. Mikhailov, M. Yu. Isaev, J. Nuehrenberg, A.A. Subbotin, W.A. Cooper, M.F. Heyn, V.N. Kalyuzhnyj, S.V. Kasilov, W. Kernbichler, V.V. Nemov, M.A. Samitov, V.D. Shafranov, Topology of magnetic field strength surfaces and particle confinement in mirror-type stellarators, in: C. Silva, C. Varandas, D. Campbell (Eds.), 28th EPS Conference on Controlled Fusion and Plasma Physics, Funchal, 18–22 June 2001, vol. 25A of ECA, European Physical Society, 2001, pp. 757–760.
[5] M.I. Mikhailov, V.D. Shafranov, A.A. Subbotin, M.Yu. Isaev, J. Nührenberg, R. Zille, W.A. Cooper, Improved α-particle confinement in stellarators with poloidally closed contours of the magnetic field strength, Nucl. Fusion 42 (2002) L23–L26.
[6] A.A. Subbotin, W.A. Cooper, M. Yu. Isaev, M.I. Mikhailov, J. Nührenberg, M.F. Heyn, V.N. Kalyuzhnyj, S.V. Kasilov, W. Kernbichler, V.V. Nemov, M.A. Samitov, V.D. Shafranov, R. Zille, Quasi-isodynamical configurations without transitional particle orbits, in: B. Duval (Ed.), 29th EPS Conference on Plasma Physics Controlled Fusion, Montreux, 17–21 June 2002, vol. 26B of ECA, European Physical Society, 2002, p. P-5.086.
[7] V.D. Shafranov, W.A. Cooper, M.F. Heyn, M. Yu. Isaev, V.N. Kalyuzhnyj, S.V. Kasilov, W. Kernbichler, M.I. Mikhailov, V.V. Nemov, C. Nührenberg, J. Nührenberg, M.A. Samitov, A.A. Skovoroda, A.A. Subbotin, R. Zille, Results of integrated optimization of $n = 9$ quasi-isodynamic stellarator, in: 31st EPS Conference on Plasma Physics London, 28 June–2 July 2004, vol. 28G of ECA, European Physical Society, 2004, p. P-4.167.
[8] G. Grieger, W. Lotz, P. Merkel, J. Nührenberg, J. Sapper, E. Strumberger, H. Wobig, W7-X Team, R. Burhenn, V. Erckmann, U. Gasparino, L. Giannone, H.J. Hartfuss, R. Jaenicke, G. Kiihner, H. Ringler, A. Weller, F. Wagner, W7-AS Team, Physics optimization of stellarators, Phys. Fluids B 4 (7) (1992) 2081–2091.
[9] A.F. Almagri, D.T. Anderson, F.S.B. Anderson, P.H. Probert, J.L. Shohet, J.N. Talmadge, A helically symmetric stellarator (HSX), IEEE Trans. Plasma Sci. 27 (1) (1999) 114–115.
[10] A. Reiman, L. Ku, D. Monticello, S. Hirshman, S. Hudson, C. Kessel, E. Lazarus, D. Mikkelsen, M. Zarnstorff, L.A. Berry, A. Boozer, A. Brooks, W.A. Cooper, M. Drevlak, E. Fredrickson, G. Fu, R. Goldston, R. Hatcher, M. Isaev, C. Jun, S. Knowlton,

M. Lewandowski, Z. Lin, J.F. Lyon, P. Merkel, M. Mikhailov, W. Miner, H. Mynick, G. Neilson, B.E. Nelson, C. Nührenberg, N. Pomphrey, M. Redi, W. Reiersen, P. Rutherford, R. Sanchez, J. Schmidt, D. Spong, D. Strickler, A. Subbotin, P. Valanju, R. White, Recent advances in the design of quasiax-isymmetric stellarator plasma configurations, Phys. Plasmas 8 (5) (2001) 2083–2094.

[11] M.C. Zarnstorff, L.A. Berry, A. Brooks, E. Fredrickson, G.Y. Fu, S. Hirshman, S. Hudson, L.P. Ku, E. Lazarus, D. Mikkelsen, D. Monticello, G.H. Neilson, N. Pomphrey, A. Reiman, D. Spong, D. Strickler, A. Boozer, W.A. Cooper, R. Goldston, R. Hatcher, M. Isaev, C. Kessel, J. Lewandowski, J.F. Lyon, P. Merkel, H. Mynick, B.E. Nelson, C. Nuehrenberg, M. Redi, W. Reiersen, P. Rutherford, R. Sanchez, J. Schmidt, R.B. White, Physics of the compact advanced stellarator NCSX, Plasma Phys. Contr. Fusion 43 (2001) A237–A249.

[12] D.A. Spong, S.P. Hirshman, L.A. Berry, J.F. Lyon, R.H. Fowler, D.J. Strickler, M.J. Cole, B.N. Nelson, D.E. Williamson, A.S. Ware, D. Alban, R. Sanchez, G.Y. Fu, D.A. Monticello, W.H. Miner, P.M. Valanju, Physics issues of compact drift optimized stellarators, Nucl. Fusion 41 (6) (2001) 711–716.

[13] D.A. Spong, S.P. Hirshman, J.F. Lyon, L.A. Berry, D.J. Strickler, Recent advances in quasi-poloidal stellarator physics issues, Nucl. Fusion 45 (2005) 918–925.

[14] V.V. Nemov, S.V. Kasilov, W. Kernbichler, M.F. Heyn, Evaluation of $1/\nu$ neoclassical transport in stellarators, Phys. Plasmas 6 (12) (1999) 4622–4632.

[15] C. Alejaldre, J. Alonso, L. Almoguera, E. Ascasibar, A. Baciero, R. Balbin, M. Blaumoser, J. Botija, B. Branas, E. de la Cal, A. Cappa, R. Carrasco, F. Castejon, J.R. Cepero, C. Cremy, J. Doncel, C. Dulya, T. Estrada, A. Fernandez, M. Frances, C. Fuentes, A. Garcia, I. Garcia-Cortes, J. Guasp, J. Herranz, C. Hidalgo, J.A. Jimenez, I. Kirpitchev, V. Krivenski, I. Labrador, F. Lapayese, K. Likin, M. Liniers, A. Lopez-Fraguas, A. Lopez-Sanchez, E. de la Luna, R. Martin, A. Martinez, M. Medrano, P. Mendez, K. McCarthy, F. Medina, B. van Milligen, M. Ochando, L. Pacios, I. Pastor, M.A. Pedrosa, A. de la Peiia, A. Portas, J. Qin, L. Rodriguez-Rodrigo, A. Salas, E. Sanchez, J. Sanchez, F. Tabares, D. Tafalla, V. Tribaldos, B. Zurro, J. Vega, D. Akulina, O.I. Fedyanin, S. Grebenshchicov, N. Kharchev, A. Meshcheryakov, R. Barth, G. van Dijk, H. van der Meiden, S. Petrov, First plasmas in the TJ-II flexible Heliac, Plasma Phys. Contr. Fusion 41 (1999) A539–A548.

[16] H.E. Mynick, N. Pomphrey, Control-matrix approach to stellarator design and control, Phys. Plasmas 7 (12) (2000) 4960–4971.

[17] H.E. Mynick, N. Pomphrey, S. Ethier, Exploration of stellarator configuration space with global search methods, Phys. Plasmas 9 (3) (2002) 869–876.

[18] S.P. Hirshman, W.I. van Rij, P. Merkel, Three-dimensional free boundary calculations using a spectral Green's function method, Comp. Phys. Commun. 43 (1986) 143–155.

[19] B. Seiwald, V.V. Nemov, V.N. Kalyuzhnyj, S.V. Kasilov, and W. Kernbichler, Optimization of neoclassical transport in URAGAN-2M, In: 31st EPS Conference on Plasma Physics London, 28 June–2 July 2004, vol. 28G of ECA, European Physical Society, 2004, p. P-5.118.

[20] S.P. Hirshman, K.C. Shaing, W.I. van Rij, C.O. Beasley Jr., E.C. Crume Jr., Plasma transport coefficients for nonsymmetric toroidal confinement systems, Phys. Fluids 29 (9) (1986) 2951–2959.

[21] W.I. van Rij, S.P. Hirshman, Variational bounds for transport coefficients in three-dimensional toroidal plasmas, Phys. Fluids B 1 (3) (1989) 563–569.

[22] A.H. Reiman, H.S. Greenside, Numerical solution of three-dimensional magnetic differential equations, J. Comput. Phys. 75 (1988) 423–443.

[23] K. Harafuji, T. Hayashi, T. Sato, Computational study of three-dimensional magnetohydrodynamic equilibria in toroidal helical systems, J. Comput. Phys. 81 (1) (1989) 169–192.

[24] Y. Suzuki, N. Nakajima, K. Watanabe, Y. Nakamura, T. Hayashi, Development and application of HINT2 to helical system plasmas, Nucl. Fusion 46 (11) (2006) L19–L24.

[25] B. Seiwald, V.V. Nemov, S.V. Kasilov, and W. Kernbichler, Optimization of stellarators with respect to neoclassical transport in real space, in: B. Duval, (Ed.), 29th EPS Conference on Plasma Physics and Controlled Fusion, Montreux, 17–21 June 2002, vol. 26B of ECA, European Physical Society, 2002, p. P–4.099.

[26] R.D. Hazeltine, J.D. Meiss, Plasma Confinement, Front. Physics, vol. 86, Addison Wesley, 1992.

[27] A.A. Galeev, R.Z. Sagdeev, Reviews of Plasma Physics, vol. 7, Consultants Bureau, New York, 1979.

[28] W. Lotz, J. Nührenberg, Monte Carlo computations of neoclassical transport, Phys. Fluids 31 (10) (1988) 2984–2991.

[29] H. Maaßberg, R. Brakel, R. Burhenn, U. Gasparino, P. Grigull, M. Kick, G. Kühner, H. Ringler, F. Sardei, U. Stroth, A. Weller, Transport in stellarators, Plasma Phys. Contr. Fusion 35 (1993) B319–B332.

[30] H. Maaßberg, C.D. Beidler, E.E. Simmet, Density control problems in large stellarators with neoclassical transport, Plasma Phys. Contr. Fusion 41 (1999) 1135–1153.

[31] K. Ida, M. Osakabe, K. Tanaka, T. Minami, S. Nishimura, S. Okamura, A. Fujisawa, K. Yamazaki, Y. Yoshimura, S. Kubo, R. Akiyama, D.S. Darrow, H. Idei, H. Iguchi, M. Isobe, S. Kado, T. Kondo, S. Lee, K. Matsuoka, S. Morita, I. Nomura, S. Ohdachi, M. Sasao, A. Shimizu, S. Takagi, C. Takahashi, S. Takayama, M. Takechi, K. Toi, K. Tsumori, T. Watari, Transition from l mode to high ion temperature mode in CHS heliotron/torsatron plasmas, Nucl. Fusion 39 (11Y) (1999) 1649–1658.

[32] O. Motojima, N. Ohyabu, A. Komori, O. Kaneko, H. Yamada, K. Kawahata, Y. Nakamura, K. Ida, T. Akiyama, N. Ashikawa, W.A. Cooper, A. Ejiri, M. Emoto, N. Ezumi, H. Funaba, A. Fukuyama, P. Goncharov, M. Goto, H. Idei, K. Ikeda, S. Inagaki, M. Isobe, S. Kado, H. Kawazome, K. Khlopenkov, T. Kobuchi, K. Kondo, A. Kostrioukov, S. Kubo, R. Kumazawa, Y. Liang, J.F. Lyon, A. Mase, S. Masuzaki, T. Minami, J. Miyazawa, T. Morisaki, S. Morita, S. Murakami, S. Muto, T. Mutoh, K. Nagaoka, Y. Nagayama, N. Nakajima, K. Nakamura, H. Nakanishi, K. Narihara, Y. Narushima, K. Nishimura, N. Nishino, N. Noda, T. Notake, H. Nozato, S. Ohdachi, Y. Oka, H. Okada, S. Okamura, M. Osakabe, T. Ozaki, B.J. Peterson, A. Sagara, T. Saida, K. Saito, S. Sakakibara, M. Sakamoto, R. Sakamoto, M. Sasao, K. Sato, M. Sato, T. Seki, T. Shimozuma, M. Shoji, H. Suzuki, Y. Takeiri, N.

Takeuchi, N. Tamura, K. Tanaka, M.Y. Tanaka, Y. Teramachi, K. Toi, T. Tokuzawa, Y. Tomota, Y. Torii, K. Tsumori, K.Y. Watanabe, T. Watari, Y. Xu, I. Yamada, S. Yamamoto, T. Yamamoto, M. Yokoyama, S. Yoshimura, Y. Yoshimura, M. Yoshinuma, N. Asakura, T. Fujita, T. Fukuda, T. Hatae, S. Higashijima, A. Isayama, Y. Kamada, H. Kubo, Y. Kusama, Y. Miura, T. Nakano, H. Ninomiya, T. Oikawa, N. Oyama, Y. Sakamoto, K. Shinohara, T. Suzuki, H. Takenaga, K. Ushigusa, T. Hino, M. Ichimura, Y. Takase, F. Sano, H. Zushi, T. Satow, S. Imagawa, T. Mito, I. Ohtake, T. Uda, K. Itoh, K. Ohkubo, S. Sudo, K. Yamazaki, K. Matsuoka, Y. Hamada, M. Fujiwara, Recent advances in the LHD experiment, Nucl. Fusion 43 (2003) 1674–1683.

[33] L.M. Kovrizhnykh, Neoclassical theory of transport processes in toroidal magnetic confinement systems, with emphasis on non-axisymmetric configurations, Nucl. Fusion 24 (7) (1984) 851–936.

[34] C.D. Beidler, W.N.G. Hitchon, W.I. van Rij, S.P. Hirshman, J.L. Shohet, Unified theory of ripple transport in stellarators, Phys. Rev. Lett 58 (17) (1987) 1745–1747.

[35] A.H. Boozer, Plasma equilibrium with rational magnetic surfaces, Phys. Fluids 24 (11) (1981) 1999–2003.

[36] V.V. Nemov, S.V. Kasilov, W. Kernbichler, and M.F. Heyn. Evaluation of an effective ripple in stellarators, in: C. Silva, C. Varandas, and D. Campbell, (Eds.), 28th EPS Conference on Controlled Fusion and Plasma Physics, Funchal, 18–22 June 2001, vol. 25A of ECA, European Physical Society, 2001, pp. 1985–1988.

[37] V.V. Nemov, Calculations of the magnetic surface function gradient and associated quantities in a torsatron, Nucl. Fusion 28 (10) (1988) 1727–1736.

[38] S. Kirkpatrick, C.D. Gelatt Jr., M.P. Vecchi, Optimization by Simulated Annealing, Science 220 (4598) (1983) 671–680.

[39] E. Aarts, J. Korst, Simulated Annealing and Boltzmann Machines, Wiley, 1989.

[40] R.V.V. Vidal (Ed.), Applied Simulated Annealing, Springer-Verlag, 1993.

[41] B. Seiwald, V.N. Kalyuzhnyj, S.V. Kasilov, W. Kernbichler, V.V. Nemov, Neoclassical transport in Uragan-2M for the $1/\nu$ regime, Fusion Sci. Technol. 50 (3) (2006) 447–456.

[42] W. Gropp, E. Lusk, User's Guide for MPICH, a Portable Implementation of MPI, Argonne National Laboratory, Mathematics and Computer Science Division (1999).

[43] MPICH webpage: <http://www-unix.mcs.anl.gov/mpi/>.

[44] C. Alejaldre, J.J.A. Gozalo, J. Botija Perez, F. Castejón Magaña, J.R. Cepero Diaz, J. Guasp Perez, A. López-Fraguas, L. García, V.I. Krivenski, R. Martín, A.P. Navarro, A. Perea, A. Rodriguez-Yunta, M. Sorolla Ayza, A. Varias, TJ-II project: a flexible heliac stellarator, Fusion Technol. 17 (1990) 131–139.